Chapter 11

45°-Tilted Fiber Gratings and Their Application in Ultrafast Fiber Lasers

Zhijun Yan, Chengbo Mou, Yishan Wang, Jianfeng Li, Zuxing Zhang, Xianglian Liu, Kaiming Zhou and Lin Zhang

Additional information is available at the end of the chapter

http://dx.doi.org/10.5772/61739

Abstract

This chapter reviews the recentachievements of 45°-tilted fiber gratings (45°-TFGs) in all fiber laser systems, including the theory, fabrication, and characterization of 45° TFGs and 45° TFG-based ultrafast fiber laser systems working in different operating regimes at the wavelength of 1 μm, 1.5 μm, and 2 μm.

Keywords: Tilted fiber grating, nonlinear polarization rotation, mode-locked fiber laser

1. Introduction

Recently, ultrafast fiber lasers giving rise to ultrashort light pulses have attracted much more attention in modern scientific and industrial communities owing to their wide applications and unique advantages, such as compact configuration, high reliability, high output power, better beam quality, and low cost. It is a complex physical mechanism to generate ultrashort pulses, which is a result of the interplay of group velocity dispersion (GVD), self-phase modulation (SPM), gain saturation, cavity loss, and higher-order dispersion in the laser cavity. Especially, in a passively mode-locked ultrafast fiber laser system, the key to achieve ultrashort output is to implement a saturated absorption mechanism (SAM) in the laser cavity. There are two main SAMs: (1) saturated absorption material-based physical intensity SAM (semiconductor- or nano-material-based saturable absorber) and (2) fiber nonlinearity-based artificial SAM (nonlinear polarization rotation (NPR), nonlinear optical loop mirror (NOLM)). Compared with the other techniques, NPR overcomes the limitation on optical damage threshold and modulation capability of those physical absorbers. In the early development stage, most of the fiber laser systems used some bulk components which greatly affected the integration

and stability and also induced extra insertion loss. With the advent of multifarious in-fiber components, fiber laser systems with all-fiber configuration are becoming possible, which have boomed the development of ultrafast fiber lasers. Moreover, fiber laser system constructed by in-fiber devices benefits from advantages such as no collimation, low insertion loss, high stability, and zero maintenance. In-fiber components are hence of critical importance for ultrafast fiber lasers in order to exhibit the above-mentioned plethora of merits. The most used in-fiber devices in a fiber laser include rare-earth doped gain fiber [1], fused silica-based in-fiber beam combiner [2], and fiber grating-based components [3–5]. In NPR technique, it is important to employ a linear polarizer to induce polarization-dependent loss in the laser cavity. As an effective in-fiber polarizer, 45°-tilted fiber grating (45°-TFG) was first reported by Zhou et al. in 2005 [6]. Compared with other commercial in-fiber polarizers, 45°-TFGs own many unique advantages such as high polarization extinction ratio (PER), broadband responsivity, low insertion loss, flexible wavelength adjustability, and simple fabrication method, and it can be adapted to most types of fiber [7].

Because of their high PER and broadband response, fiber lasers constructed using 45°-TFGs exhibit desirable features, including high signal-to-noise ratio (SNR), good stability, and particularly high degree of polarization (DOP) output laser beam. The first trial of using a 45°-TFG as an in-fiber polarizer in fiber laser application was demonstrated by Mou et al. in 2009 [8], in which the grating was applied to achieve a single polarization continuous wave (CW) output with high DOP (>99%). Use of a 45°-TFG as the main functional device to achieve mode-locked fiber laser was reported in 2010 [9]. To date, several types of pulsed fiber laser systems utilizing 45°-TFGs with various operation regimes and wavelength ranges have been reported, which are listed in Table 1.

Year	Achievements	Authors	References
2010	Conventional soliton pulse with 600 fs duration, ~1 nj output pulse energies and 10.34 MHz repetition rate in passively mode-locked erbium-doped fiber laser	Mou et al.	[9]
2012	Dissipative soliton pulse with 4 ps duration, 29.5 MHz repetition in normal-dispersion passively mode-locked ytterbium-doped laser at 1 μm	Liu et al.	[10]
2013	Bound dissipative pulse with 5.7 ps duration and 29.6 MHz repetition rate in the all-normal dispersion mode-locked ytterbium-doped fiber laser	Liu et al.	[11]
2013	Stretched pulse with 90 fs duration, 1.68 nJ pulse energy, and 47.8 MHz repetition rate in passively mode-locked erbium-doped fiber laser	Zhang et al.	[12]
2014	Conventional soliton pulse with 2.2 ps duration, 74.6 pJ pulse energy, and 1.902 MHz repetition rate in mode-locked Thulium-doped fiber laser	Li et al.	[13]
2015	Single polarization, dual-wavelength mode-locked Yb-doped fiber laser	Liu et al.	[14]
2015	Dissipative soliton pulses with 96.7 fs duration and 251.3 MHz repetition rate in passively mode-locked erbium-doped fiber laser	Zhang et al.	[15]

Table 1. List of 45°-TFG-based all-fiber mode-locked laser systems

http://dx.doi.org/10.5772/61739

This chapter will review the theory, fabrication, and characterization of 45°-TFGs and their applications in all fiber mode-locked laser systems. The chapter will include three main parts. The first part will give a general introduction and fundamental background on the development of 45°-TFGs with a particular emphasis on fiber laser applications; second, the theory, fabrication, and characterization of 45°-TFGs will be discussed; finally, 45°-TFG-based mode-locking fiber laser systems will be reviewed including mode-locked fiber laser working at different operation regimes [9, 12, 15] and mode-locked fiber lasers operating at the wavelength ranges of 1 μm, 1.5 μm, and 2 μm [10, 13].

2. Theory, fabrication, and spectral characteristics of 45°-TFGs

Ultraviolet (UV)-inscribed fiber grating devices that have been mostly developed during the last two decades show many advantages, such as simple and mature fabrication process, wide availability in a range of optical fibers and broad operating wavelength range from visible to mid-IR [16]. The periodic structure of a fiber grating offers unique function to control light from the forward propagating core mode into the backward propagating core/cladding modes or to the forward propagating cladding and radiation modes, depending on the grating structure. As a mature technique, UV inscription has been used for producing many types of in-fiber grating devices, including standard fiber Bragg grating (FBG)-based reflectors [17], chirped fiber Bragg grating (CFBG)-based dispersion compensator [18], long period grating (LPG)-based mode convertor [19], and tilted fiber grating (TFG)-based polarizer and polarization-dependent loss equalizer [20].

2.1. Theory

The tilted fiber grating with asymmetric structure can induce high polarization-dependent mode coupling among core, cladding, and radiation modes. The 45°-TFG allows strong coupling of *s*-polarization (TE) from the forward propagating core mode into radiation modes, while the residual *p*-polarization (TM) light propagates along the fiber core with a minimal loss, which forms an ideal in-fiber polarizer. The physical principle behind this phenomenon may be well explained by the Brewster's law. As we know, the light incident at Brewster's angle on an optical interface will partially cease its TE component. In a typical UV-inscribed fiber grating structure, the UV-induced refractive index modulation is very small ($\Delta n \sim 10^{-1}$), far less than the index of fiber core. The Brewster angle for a UV-inscribed grating plane may be calculated as $\theta_{\text{Brewster}}=\arctan(n_{\text{core}}/(n_{\text{core}} + \Delta n)) \cong 45°$. Thus, when the grating structure inscribed into a fiber core at 45° with respect to the normal of fiber axis could be regarded as a series of optical interfaces at Brewster's angle, the grating will totally radiate TE light out from the fiber core, similar to the pile-of-plate polarizer, acting as an in-fiber polarizer (Figure 1).

In ref. [6], the transmission spectra of TFGs with various tilting angles for TE and TM light have been simulated (see Figure 2). The transmission loss of TM is almost zero, when the tilted angle of grating is at 45°.

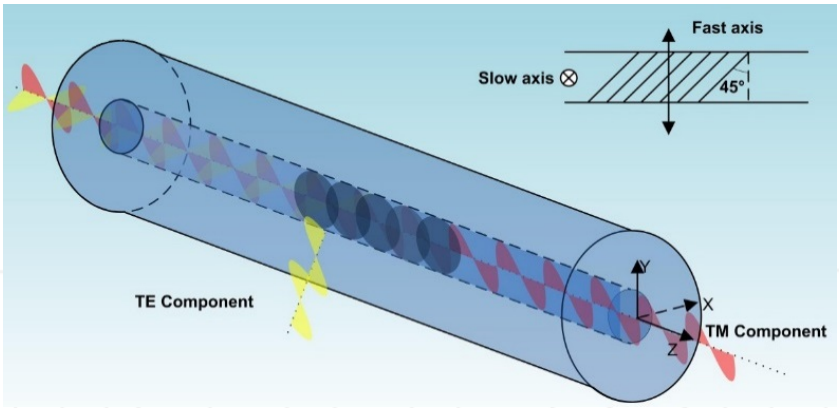

Figure 1. Schematic of 45°-TFG-based in-fiber polarizer.

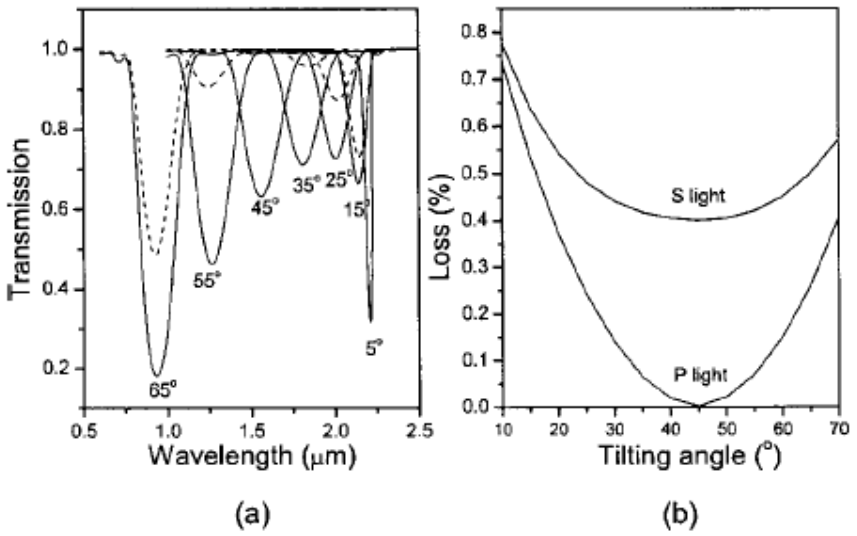

Figure 2. (a) Simulated transmission spectra of TFGs with various tilting angles. TM-light (dashed curves); TE-light (solid curves); (b) simulated transmission losses of TFGs versus tilting angles for *s*-light (TE) and *p*-light (TM). The peak wavelength is set as 1.55 μm and the grating period is varied accordingly[6].

2.2. Theoretical analysis of 45°-TFG

2.2.1. Phase matching condition

The phase matching condition (PMC) originates from the conservation of momentum, which provides a clear way to understand the mode coupling mechanism of the fiber grating. Under

http://dx.doi.org/10.5772/61739

PMC, the energy of one mode in the optical fiber can be transferred to another mode by a fiber grating structure. The general vector expression of PMC of a fiber grating can be written as follows:

$$\begin{aligned} &\vec{K}_x = \vec{K}_{\text{core}} + \vec{K}_{\text{G}} \\ &\vec{K}_x = n_x \frac{2\pi}{\lambda};\ \vec{K}_{\text{core}} = n_{\text{core}} \frac{2\pi}{\lambda};\ \vec{K}_{\text{G}} = n_{\text{core}} \frac{2\pi}{\Lambda} \cos\theta \end{aligned} \tag{1}$$

where subscript x represents core/cladding/radiation mode, θ is the tilt angle of fiber grating, n_{core} is the refractive index of the fiber core.

In Equation 1, the refractive index difference between fiber core and cladding could be neglected due to the weakly guiding condition. Hence, the strongest coupling wavelength of a 45°-TFG occurs at

$$\lambda_{\text{strongest}} = \frac{n\Lambda_{\text{G}}}{\cos 45°} \tag{2}$$

where n is the modal index of fundamental core mode and Λ_{G} is the normal period of the grating.

2.2.2. Numerical simulation of 45°-TFG

So far, there are three main theories that can be used to simulate the TFG spectral response: (1) coupled mode theory (CMT) [21, 22], (2) volume current method (VCM) [23], and (3) beam tracing method (BTM)[24]. Each method has its own pros and cons: BTM is the simplest method and better understood by the readers, but it only gives a rough estimation, because the impact of the waveguide structure has been ignored in this method; CMT is more accurate, but the simulation procedure can be quite complex, and analytical solutions are usually required. Above all, VCM is a better method especially in calculation of the distribution of radiation modes in the near and far fields a 45°-TFG, although from which the cladding boundary of waveguide is neglected. These distributed radiation modes are of great interest due to the intrinsic mode-coupling feature from the tilted fiber grating structure. From VCM theory, the loss coefficient per unit length of a 45°-TFG can be expressed as follows [6, 23]:

$$\begin{aligned} \alpha = &-\frac{k_{\text{o}}{}^3 \delta n^2}{4n\left(1 + \left(\frac{u^2}{w^2}\right)\right)} \frac{K_1{}^2(aw)}{K_0{}^2(aw)} \oint [1 - \sin^2\xi \cos^2(\chi - \phi)] \\ &\times \left[\frac{R_{\text{s}} J_0(au) J_1(aR_{\text{s}}) - u J_0(aR_{\text{s}}) J_1(au)}{R_{\text{s}}{}^2 - u^2}\right]^2 d\phi \end{aligned} \tag{3}$$

where $k_0 = 2\pi/\lambda_0$ is the wave vector of light in vacuum, δn and n are the modulated and original refractive indices of the fiber core, a is the core radius and u and w are the waveguide parameters, J and K are the first kind Bessel function and the second kind modified Bessel function, respectively.

In Equation 3, $R_s = (R_t^2 + k_0^2 n_{cl}^2 \sin\xi^2 + 2R_t k_0 n_{cl} \sin\xi \times \cos\varphi)^{1/2}$, where ξ is the angle between the radiation beam and the fiber axis, which satisfies $R_g - i_{eff} k_0 + k_0 n_{cl} \cos\xi = 0$; χ denotes the polarization of the core mode; R_t and R_g are wave vectors of grating along the fiber axis and across the fiber cross section and are defined as $R_t = 2\pi/\Lambda_g \sin 45°$ and $R_g = 2\pi/\Lambda_g \cos 45°$, where Λ_g is the period of grating.

For a specific type of fiber, the waveguide parameters of fiber are fixed; thus the loss coefficient per unit length will solely depend on the UV-induced index change and azimuthal angle of polarization state. So, the transmission loss of a 45°-TFG may be calculated as follows:

$$T = \mathrm{Exp}\left(-\alpha\left(\phi,\ \delta n, \lambda\right) * l\right) \tag{4}$$

where l is the length of grating, λ is the wavelength of incident light, and φ denotes the polarization state of incident light. According to the coordinator system in the analysis, when $\varphi = 0^0$, T represents the transmission loss of TM polarization light; when $\varphi = 90^0$, T represents the transmission loss of TE polarization light.

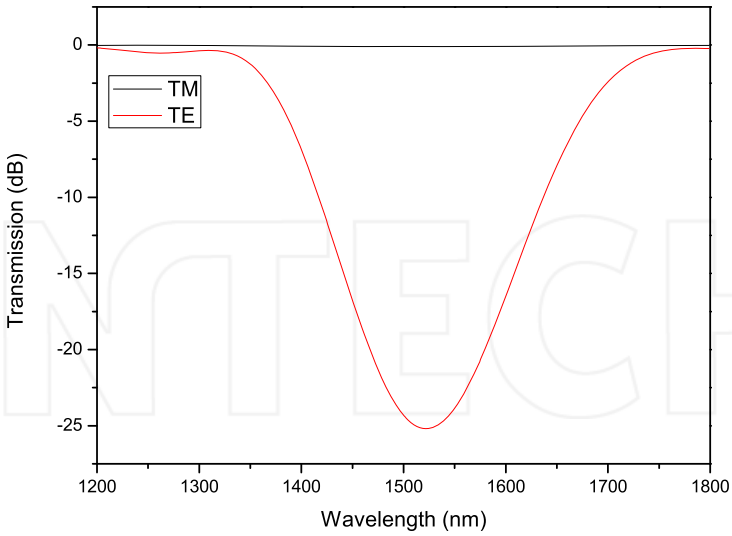

Figure 3. The simulation results of the transmission loss against the wavelength for TM polarization (black line) and TE polarization (red line) of a 45°-TFG with 24-mm length [7].

http://dx.doi.org/10.5772/61739

Figure 3 displays the simulated transmission spectra of a 45°-TFG with 24-mm length, which clearly shows that the TM polarization light has near-zero loss when passing through the 45°-TFG, while the TE polarization light has a very broad loss band with a maximum loss of 27 dB at 1520 nm. In the simulation, the fiber parameters were set the same as the SMF-28 single-mode fiber; the period and the length of grating, and the refractive index modulation were 748 nm, 24 mm, and 0.0013, respectively.

2.2.3. The design of tilt angles

In contrast to the inscription of FBG, the interference fringes of UV beam are tilted at an angle with respect to the fiber axis during the inscription of TFGs. Due to the cylindrical shape of optical fiber, the tilt angle of the interference fringes outside of the fiber is different from that inside of the fiber, as depicted in Figure 6.

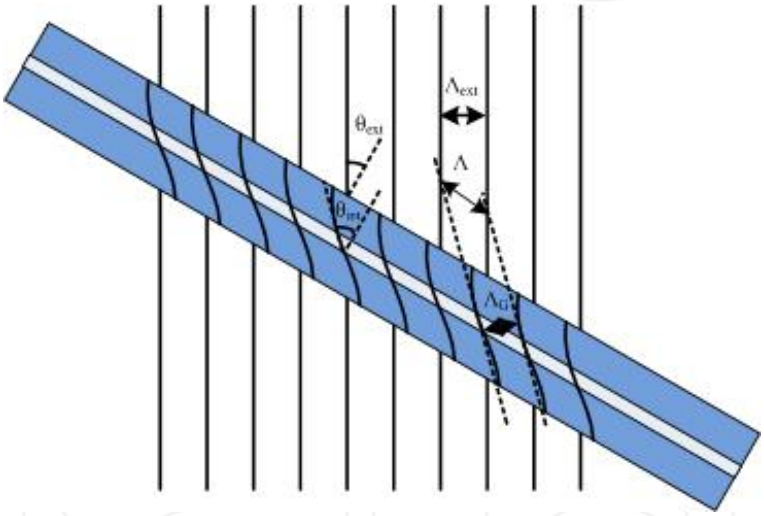

Figure 4. Illustration of fringes of a TFG outside and inside of the fiber with external angle θ_{ext} and internal angle θ_{int}.

The relationship between θ_{ext} and θ_{int} is given by ref. [29] as follows:

$$\theta_{int} = \frac{\pi}{2} - \tan^{-1}\left[\frac{1}{n_{UV}\tan(\theta_{ext})}\right] \tag{5}$$

where n_{UV} is the refractive index of the fiber at wavelength of UV laser (here, it is around 1.52). According to Equation 4, to inscribe 45°-TFGs, the tilted angle of interference pattern outside the fiber is 33.7° with respect to the fiber axis. As shown in the relation between the period of internal interference fringe and external fringe can be given as:

$$\Lambda = \frac{\Lambda_{ext}}{\cos\theta_{ext}} = \frac{\Lambda_G}{\cos\theta_{int}} \tag{6}$$

where Λ_G and Λ_{ext} are the periods of grating and the UV interference fringes, respectively, and Λ_{ext} is half of the period of phase mask (Λ_{PM}). The relationship between the strongest coupling wavelength of a 45°-TFG and the period of phase mask is given as follows:

$$\lambda_{strongest} = \frac{n\Lambda_{PM}}{2\cos 33.7^{\circ}} \tag{7}$$

2.3. Fabrication of 45-TFGs

There are three main grating fabrication methods: two-beam interferometric technique (holographic method)[25], point-by-point inscription [26], and phase mask scanning technique [27, 28]. Among them, due to the limitation of UV beam size, the point-by-point technique is not suited for short-period grating inscription, the holographic method has the grating length limitation, and only the phase-mask scanning technique is more suitable for the fabrication of longer and stronger 45°-TFGs. A typical 3-D schematic of the grating inscription system is shown in Figure 4, which includes a 244-nm CW frequency doubled Ar+ laser with computer-controlled high-precision air-bearing stage. The phase mask used for 45°-TFG fabrication has 33.7° tilted pattern with respect to the fiber axis, so as to make sure the grating pattern inside of the fiber core will have a 45° tilt angle [7].

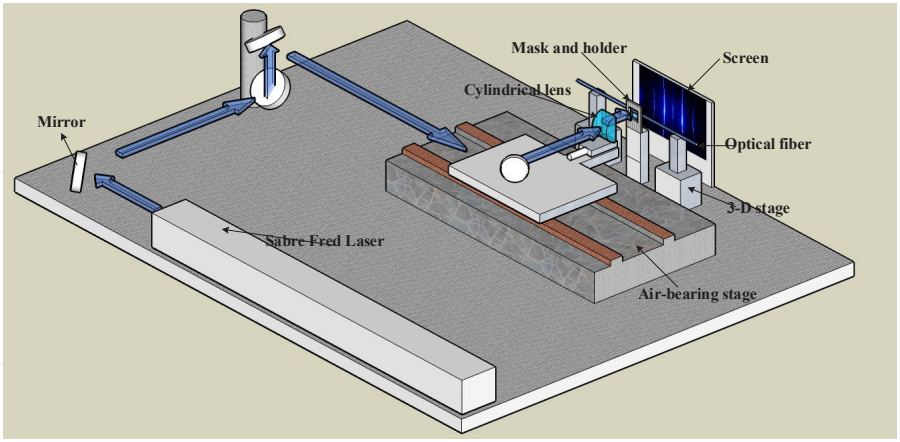

Figure 5. Typical fiber grating inscription system using the phase-mask scanning technique

To enhance the photosensitivity of standard single-mode fiber, the fiber samples are usually hydrogen loaded at 150 bar at 80°C for two days. The phase mask for inscribing 45°-TFG has

http://dx.doi.org/10.5772/61739

a uniform pitch and 33.7° tilted angle with respect to the fiber axis (can be purchased from Ibsen Photonics). For standard FBGs with 30-mm length, a very small refractive index modulation (~10^{-4}–10^{-5}) can produce 40-dB reflectance. However, for 30-mm-long 45°-TFGs, to achieve 40 dB PER, the refractive index modulation induced by UV beam needs to be greater than 10^{-3}. The refractive index modulation level depends on the intrinsic photosensitivity of fiber and the UV exposure condition. For normal nonphotosensitive fiber, to induce higher index modulation, the fiber needs to be exposed under high dose of UV radiation for longer time. Figure 5 shows the micro-image of a 45°-TFG inscribed into SMF-28 single-mode fiber with 8.65-μm fiber core diameter. Ten pitch periods of the grating is 7.59 μm, which indicates the central response wavelength of this 45°-TFG is at ~1550 nm.

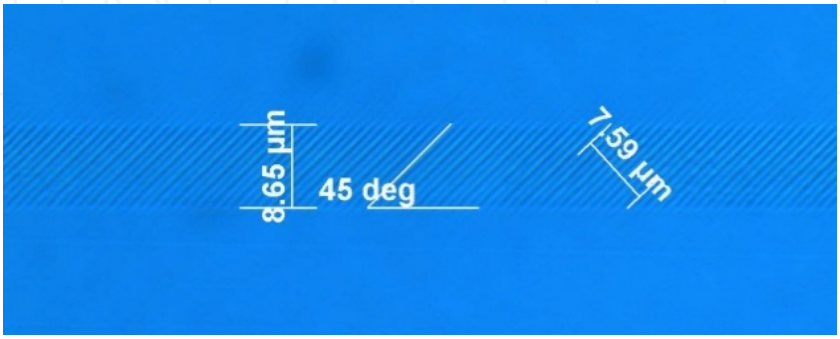

Figure 6. The micro-image of the grating structure of a UV-inscribed 45°-TFG in SMF-28 fiber

2.4. PER characterization

As a polarization-dependent device, the PER is a key parameter to be evaluated for a 45°-TFG, which is the peak-to-peak difference in transmission with respect to all possible states of polarization [30]. Quantitatively, the PER is the ratio of the transmission with respect to all polarization states. For a 45°-TFG, the PER is the ratio of the transmission of the TM and TE polarization states, which can be expressed as follows:

$$\mathrm{PER} = 10 \times \log \frac{T_{\mathrm{TM}}}{T_{\mathrm{TE}}} = 10 \times l\left(\alpha(0°) - \alpha(90°)\right)\log(e) \tag{8}$$

From Equations 3 and 9, the PER of 45°-TFG is linearly proportional to the length of grating and the square of index modulation.

As an ideal in-fiber polarizer, the PER, operation bandwidth, and output polarization state are very important parameters. The typical experimental setup for measuring PER is shown in Figure 7, which usually consists of a light source, a power meter (or an optical spectrum analyzer), and a commercial fiber polarizer and polarization controller (PC). The light source

is usually a single-wavelength source; the polarizer is used to generate polarized light with a high degree of polarization (it is not necessary to use a polarizer, if the light source gives out polarized light) and the PC is employed to change the polarization state for the output. The maximum and minimum transmission through the component can directly be measured using this system by adjusting PC. The PER can then be calculated using Equation 9.

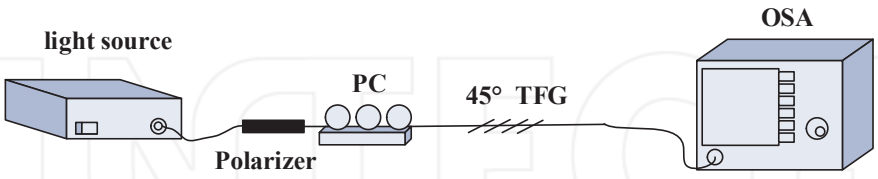

Figure 7. The experiment setup of PER measurement

Figures 8 (a) and (b) show the typical PER results of a 24-mm-long 45°-TFG measured by the difference of maximum and minimum transmission loss using a 1530-nm single-wavelength laser with respect to all polarization states. It can be seen from these figures that the entire PER profile is near-Gaussian-like and covers a broad wavelength range. During the fabrication, one may observe that under the same UV inscription condition, the PER increases monotonically with the grating length. Figure 8(c) plots the PERs of four 45°-TFGs with different lengths (5, 15, 24, and 48 mm), clearly showing that the PER is near-linearly proportional to the grating length, which is in good agreement with previous numerical analysis. The degree of linear polarization of a 45°-TFG can be evaluated by measuring its polarization distribution. Figure 8(d) shows the polarization distributions for three 45°-TFGs with PERs of 10 dB, 20 dB, and 40 dB and a bare fiber for comparison. As shown in the figure, the higher the PER, the lower the output power at the azimuth angles of 90° and 270°, and a strong 45°-TFG has a near-perfect figure of "8" shape with a very narrow waist indicating an ultra-high PER, while the bare fiber gives a circular shape without showing any polarization dependency.

3. 45°-TFG-based all-fiber ultrafast laser systems

Ultrafast fiber laser is defined as the pulsed laser with duration from picoseconds to femtoseconds that are usually derived from a mode-locked fiber laser. Mode-locked fiber laser could be sorted as active and passive mode locking. The former relies on a physical phase modulator and the latter utilizes a saturable absorption mechanism-based modulation, from which the high-intensity pulse center experiences low loss while the low-intensity pulse wing experiences high loss. Passive mode-locking techniques are efficient to generate ultrafast pulses, simply due to the fast perturbation of the cavity. The ultra-short pulses result from the interaction of various physical effects, including GVD, SPM, saturable gain, filtering effect, and cavity loss. By using an artificial saturable absorber, the NPR-based mode-locked fiber laser was first demonstrated by K.Tamura in 1992 [32].

http://dx.doi.org/10.5772/61739

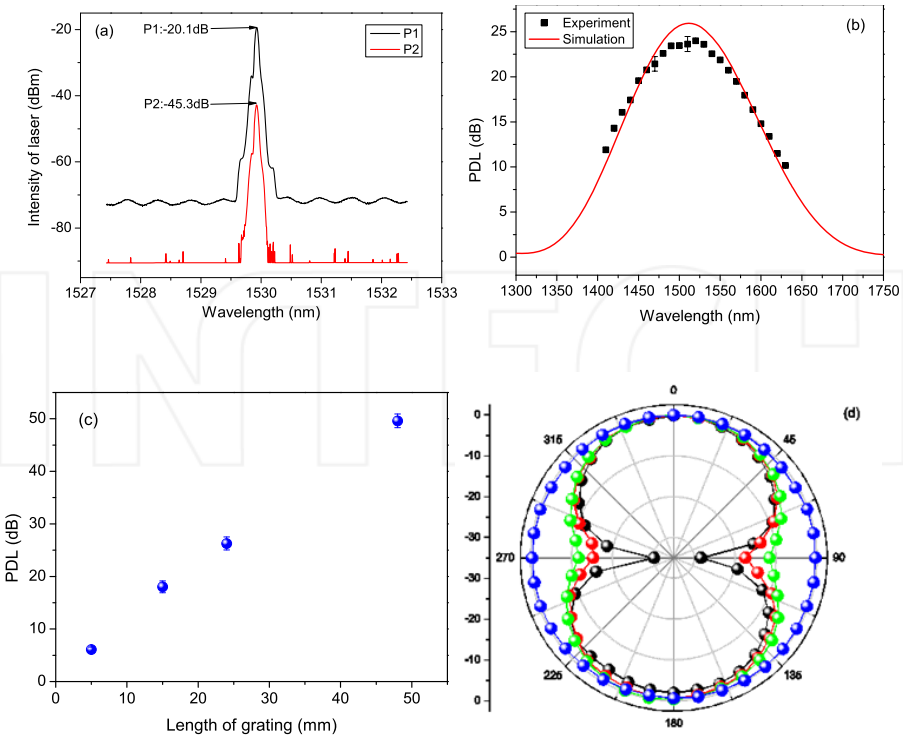

Figure 8. (a) The transmission spectra of a 45°-TFG based in-fiber polarizer at 1550nm at two orthogonal polarization states (P1 and P2); (b) the PER response of a 45°-TFG over 90nm from 1520nm to 1610nm; (c) the PER response of 45°-TFG with different grating length at 153onm; (d) the polarization distribution profiles for three 45°-TFGs with ● (green) 10dB PER, ● (red) 20 dB PER and ● (black) 40 dB PER and a bare fiber with ● (blue) 0dB PER [31].

3.1. NPR effect

In a more physical description, NPR can be regarded as the "interference" of right- and left-hand circular polarization light experiencing different nonlinear phase shifts induced by Kerr effect. The working principle of NPR is similar to that of nonlinear optical loop mirror(NOLM) both of them are based on interference between two non-equal intensity light beams that induce different nonlinear phase shifts. The phase shift in NOLM is induced from a non-balanced coupler, while in NPR it is generated from an elliptical polarization light, which resolves into two orthogonal circularly polarized components with different intensities. The NPR-based configuration usually consists of a linear polarizer and two PCs, in which the transmission intensity through the linear polarizer will be power dependent.

In the NPR-based laser system, a linear polarizer is a critical element. So far, there are two types of commercial in-fiber linear polarizer: (1) the evanescent field coupling-based in-fiber linear polarizer which is made by coating the exposed guiding region with a birefringent material (TM pass polarizer) [33], or a metal film (TE pass polarizer) [34], or an anisotropic

absorption material (TM pass polarizer) [35]; (2) polarizing fiber-based linear polarizer which is actually a high birefringence polarization-maintaining fiber [36]. Both types of in-fiber polarizer have been applied to construct mode-locked fiber lasers [37]. Recently, a picosecond mode-locked fiber laser has been reported using a micro-fiber-based polarizer [38]. However, all these types of in-fiber polarizers have their intrinsic disadvantages, such as low power tolerance, complex fabrication process for evanescent field absorption-based in-fiber polarizer, and long fiber requirement and narrow operation bandwidth and limitation of operation fiber type. As aforementioned, a 45°-TFG is an ideal in-fiber polarizer, and it can overcome the most disadvantages associated with the two mentioned conventional types of polarizer. In this section, a detailed review of recent achievements in 45°-TFG-based all-fiber ultrafast fiber lasers will be given.

The most reported mode-locked fiber lasers using 45°-TFGs are based on a common ring laser cavity structure as shown in Figure 9, in which the pump laser is combined into laser cavity by a fiber combiner; the gain fiber could be chosen to ytterbium-/erbium-/thulium-doped fiber to achieve different operation wavelengths; a 90/10 optical coupler (OC) is employed to couple out the laser light; a 45°-TFG is sandwiched between two PCs (three different period 45°-TFGs should be used for ytterbium-/erbium-/thulium-based fiber systems, respectively); polarization-independent isolator is used to achieve unidirectional operation.

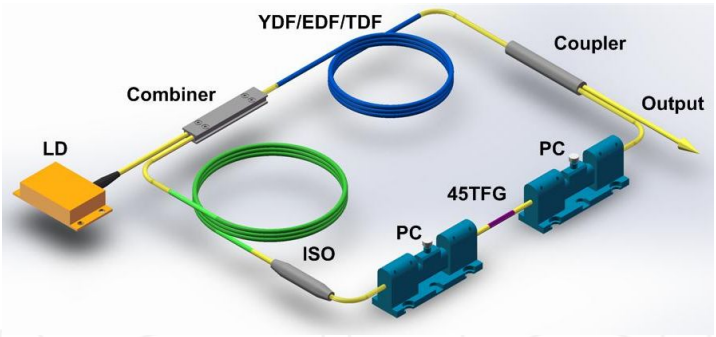

Figure 9. The configuration of a ring fiber laser cavity.

3.2. 45°-TFG-based mode-locked fiber laser at 1.5 μm

The mode-locked fiber laser in the 1.5-μm region is very important due to the potential applications in modern optical fiber communication and microwave photonics, which is also a convenient experimental platform for nonlinear science research because of wide availability of various components and types of fibers at 1.5 μm. Based on different cavity dispersion mappings, the mode-locked fiber laser could operate in the regime of conventional soliton, the stretched pulse, the similariton, and the dissipative soliton, and operating in this regime depends on the net cavity dispersion (anomalous or normal dispersion). So far, 45°-TFG-based mode-locked fiber lasers at 1.5 μm have been demonstrated as the conventional solitons, the

http://dx.doi.org/10.5772/61739

stretched pulses, and the dissipative solitons, which will be described in detail in the following sessions.

3.2.1. Conventional soliton pulse mode-locked fiber laser

One of the features of conventional soliton pulses is that they preserve their shape during propagation over very long distance and the pulses are still reproducible even after various perturbations, which have been used in a range of applications. The generation of conventional soliton pulses results from the balance of nonlinearity and dispersion. The first NPR-based soliton mode-locked fiber ring laser was reported by Tamura in 1992 [32]. The first 45°-TFG-based soliton fiber mode-locking laser was demonstrated in 2010 [9], in which the ring laser cavity consists of an ~6-m erbium-doped fiber (EDF) with nominal absorption coefficient of ~12 dB/m at 1530 nm and nominal dispersion –8.6 ps/nm/km, a 12-m SMF-28 fiber with an anomalous dispersion of ~+18 ps/nm/km, and a 0.5-m B/Ge fiber with dispersion of ~+10 ps/nm/km. The net cavity GVD of the cavity is around –0.0143 ps^2, which guarantees the laser working at soliton regime. The mode-locked short pulses can be achieved by properly adjusting the two PCs in the cavity (shown in Figure 9).

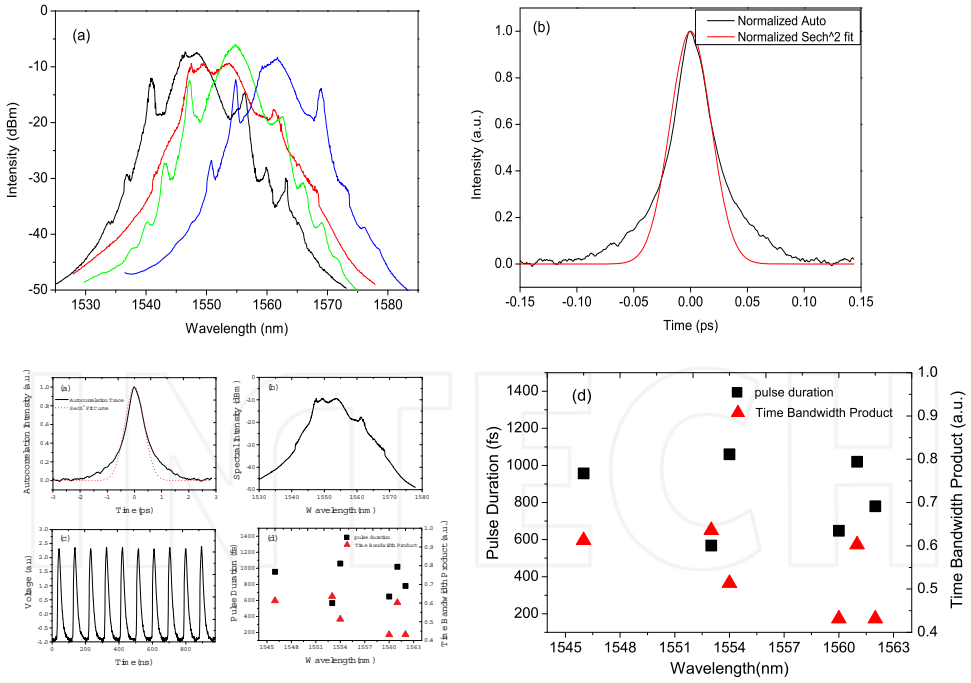

Figure 10. Measured characteristics of 45°-TFG-based all-fiber soliton mode-locking laser: (a) optical spectra of mode-locked fiber laser under different polarization status; (b) recorded autocorrelation trace; (c) output pulse train; and (d) pulse width and time-bandwidth products as a function of the wavelength [9]

Figure 10(a) shows the spectra of stable soliton pulse at different central wavelengths, from which we can observe the Kelly sidebands on the spectrum that are caused by periodic perturbation during the cavity trip. The stable soliton pulses can only be sustainable at relatively low pump power. With the increasing pump power, the pulses become unstable, and the Kelly sideband becomes much stronger. Figure 10(b) shows that the pulse duration of soliton mode-locking laser at the central wavelength of 1553 nm is ~600 fs. The pulse train was recorded by an oscilloscope as shown in Figure 10(c), which indicates the pulse separation is ~90 ns and the repetition rate is calculated around 11.1 MHz, which agrees very well with the value calculated from the total cavity length (18.5 m). Figure 10(d) shows the duration and time–bandwidth product (TBP) of soliton pulses at different central wavelengths. In the experiment, 12 mW average output power was obtained giving an ~1-nJ peak pulse energy [9].

3.2.2. Stretched pulse mode-locked fiber laser

Most important applications of ultrafast lasers are the supercontinuum generation and micromachining. The high-energy ultrashort pulses are preferred in these applications. However, the periodic perturbation for solitons may limit the duration of pulse and energy scalability. Using low anomalous dispersion fiber could overcome the periodic perturbation-induced pulse instability, but the low anomalous dispersion fiber limits the pulse energy [39]. To overcome these restrictions, one of the most efficient methods is to construct laser cavity with both normal and anomalous GVD segments, in which the pulses will be compressed at the normal GVD segment and broadened at the anomalous GVD segment. Such pulses experience something like the soliton "breathing" during the cavity round trip, so they are also called as stretched pulses [40]. In 2013, Zhang et al. reported a sub-100-fs stretched pulse by using a 45°-TFG-based ring laser system [12]. The configuration of this laser is similar to the one in Figure 9, which has a net cavity GVD of ~0.013 ps^2, contributed by an ~1.16-m EDF with nominal absorption coefficient of ~80 dB/m at 1560 nm and normal dispersion ~–53.4 ps/nm/km, 2.65-m SMF-28 fiber with anomalous dispersion ~18 ps/nm/km and 0.43 m HI1060 fiber with anomalous dispersion ~5.5 ps/nm/km.

Similarly, the mode locking in Zhang's laser was achieved by adjusting the PCs in the cavity. The pulse duration was measured by a commercial optical autocorrelator with <1 fs resolution, and the result shows an ~90-fs Gaussian fit trace (see in Figure 11(a)). From Figure 11(b), we see ~54 nm pulse spectra centered at 1575 nm that gives a TBP of ~0.58, indicating that the compressed Gaussian pulse is a little beyond the transform limit. From Figure 11(b), it is also noticed that the output spectra from the different ports have almost the same profile and width. Figures 11(c) and (d) show the pulse train is with an ~21-ns interval between two adjacent pulses and mode-locked pulse laser has a fundamental repetition rate of ~47.8 MHz, which are in good agreement with the 4.24-m cavity length. The 55-dB SNR shows that the mode-locked laser is working at a stable state [12]. It is also believed that with further optimization of the cavity parameters, shorter pulse duration could be obtained.

http://dx.doi.org/10.5772/61739

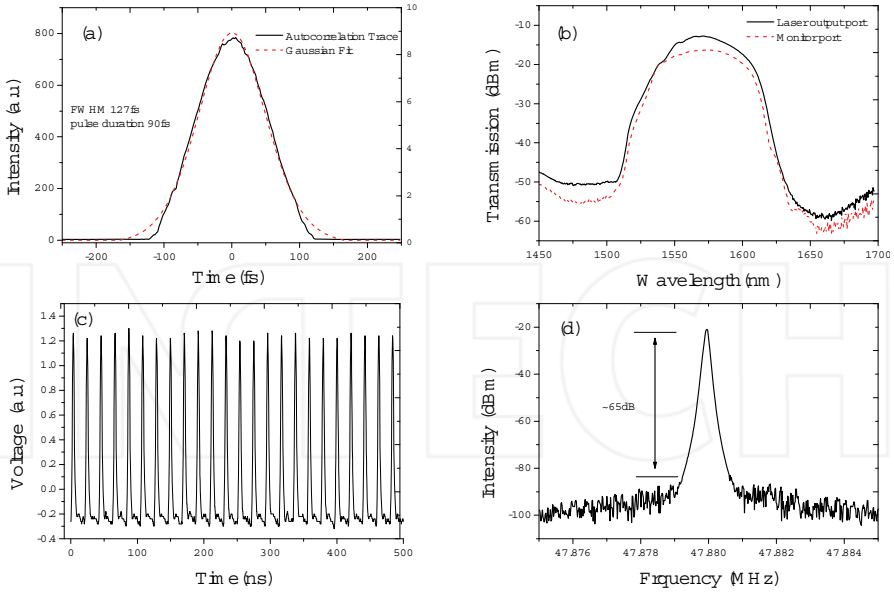

Figure 11. Characterization of 45°-TFG-based stretched pulse laser: (a) autocorrelation trace (black line) and its Gaussian fitting (red dotted line); (b) optical spectra of both output (black line) and monitor (red dotted line) ports; (c) pulse trains; (d) RF spectrum[12]

3.2.3. Dissipative soliton pulse mode-locked fiber laser

In theory, the generation of the dissipative soliton pulse is not only the balance of nonlinearity and dispersion but also the balance between gain and loss. The concept of dissipative soliton is thought as a fundamental extension of conventional soliton theory. However, there is a significant difference between conventional solitons and dissipative solitons, as the latter owns a nonuniform phase, whereas the phase of the former is constant. The nonuniform phase of dissipative pulses is caused by the fact that solitons continually exchange energy with the environment [41]. In contrast to the conventional solitons, dissipative solitons are largely positively chirped with high pulse energy. Adapting external cavity compression, <100 fs duration is easily achieved.

In 2015, Zhang et al. demonstrated a 250-MHz high fundamental repetition rate dissipative soliton laser using a 5-cm-long 45°-TFG as an intra-cavity mode locker [15]. The total cavity length of this laser is around 0.8 m, which is constituted by a 0.3-m-long EDF with normal dispersion ~–53.4 ps/nm/km at 1560 nm and peak absorption of around 150 dB/m at 1530 nm used as the gain medium, and 0.5-m SMF-28 fiber included 5-cm-long 45°-TFG with anomalous dispersion ~18 ps/nm/km. The net GVD of the laser cavity is ~0.009 ps^2. Two 976 nm laser diodes combined via a polarization beam combiner are injected into the pump port to generate enough nonlinearity. When pump power was greater than 700 mW, the stable, self-start dissipative soliton mode locking was achieved by adjusting the PCs to an appropriate

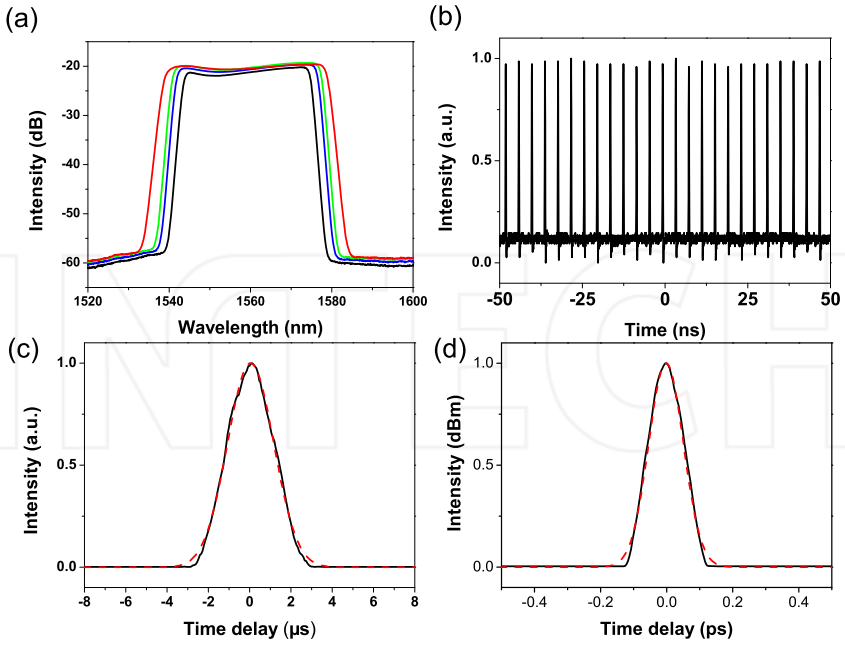

Figure 12. (a) Output spectra at different pump powers; (b) pulse train of the mode-locked pulses, (c) and (d) autocorrelation traces before and after out-cavity compression (red dashed lines are Gaussian fitting)[15].

polarization state. When the pump power was <700 mW, the laser was operating at a Q-switching regime. As shown in Figure 12(a), the full width at half maximum (FWHM) of output pulse spectra is around 37.5 nm and with increasing pump power, the FWHM of the spectra becomes broader. At 900 mW, maximal pump power, the 3-dB spectral bandwidth reaches to 41.2 nm. During the whole pump power range, no multiple pulse phenomena occurred. Once the mode-locked pulse has been generated, the laser was stable and the average output power was 43.4 mW. The output pulse train was measured by an oscilloscope, which has shown 4 ns pulse interval and 250 MHz repetition rate which agree very well with the values calculated from the cavity length (see in Figure 12 (b)). The pulse duration was measured by autocorrelation and assumed from Gaussian fitting, showing the durations were 1.8 ps and 96.7 fs before and after out-cavity compression with SMF, respectively. The obtained results were limited by the available pump power; it is expected that with higher pump power, high repetition rate fiber laser system up to GHz with increased output and shortened pulse width may be achievable.

3.3. 45°-TFG-based YDF mode-locked fiber laser at 1 μm

Ytterbium-doped fiber (YDF) has a number of interesting properties, such as simple electronic level structure, less quantum defect, upper-state lifetimes, and relative broad gain bandwidth

http://dx.doi.org/10.5772/61739

[42, 43]. Such properties potentially allow YDF-based laser systems to have very high slope efficiency, low thermal effect, high output power, and ultrashort pulses. YDF-based laser systems have been widely applied in micro-machining area due to their high photon energy, extra high power output, easy beam delivery, and a robust setup. In contrast to the EDF-based laser system, both active and passive fibers at the 1-μm region have normal dispersion. Recent research has reported that the hollow core fiber has an anomalous dispersion at ~1 μm and been employed in a laser cavity to achieve dispersion management [44]. By using the NPR technique, ultrashort, self-starting mode-locking laser operating at ~1-μm region could be achieved by using YDF and 45°-TFG. According to the phase matching condition, 45°-TFG could also work at 1-μm region by properly designing the period of tilted grating. Figure 13(a) shows the transmission spectra of a 50-mm-long 45°-TFG with 563 nm pitch period at two orthogonal polarization states at 1055.7 nm. The PER of 45°-TFG is quite high, at around 34.9 dB at 1055.7 nm. Figure 13(b) shows the simulated full PER profile of a 45°-TFG at the central wavelength of 1 μm, in which the FWHM is around 180 nm that is far broader than the gain bandwidth of YDF.

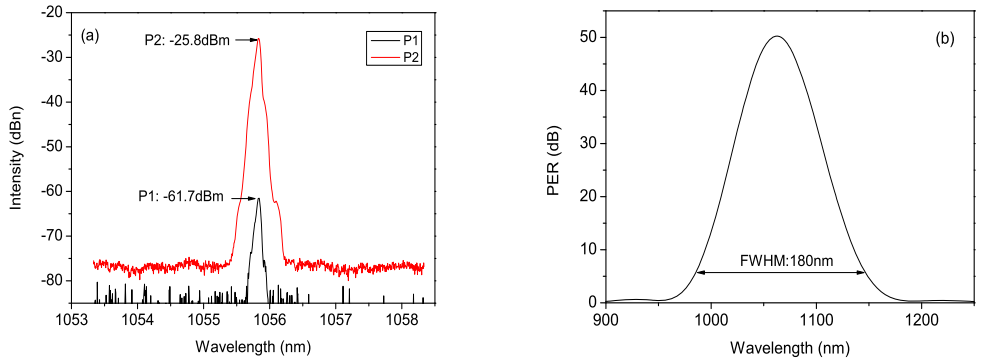

Figure 13. (a) The measured transmission spectra of a 45°-TFG-based in-fiber polarizer at 1055.7 nm at two orthogonal polarization states (P1 and P2); (b) the simulation result of a 50-mm-long 45°-TFG with 568 nm period and 0.0013 index change.

3.3.1. Dissipative soliton mode-locked fiber laser

In 2012, Liu et al. for the first time demonstrated a 45°-TFG-based all-fiber normal-dispersion mode-locked laser at the 1-μm region [10]. In this system, a 48-mm-long 45°-TFG with 33 dB PER at 1040 nm was used to build up NPR mechanism and generate dissipative soliton pulses. The all-fiber laser structure was based on a ring cavity oscillator (similar to the one in Figure 9), in which the total laser cavity length was 7 m including 0.7-m-long YDF with an absorption coefficient of 500 dB/m at 976 nm and 20 ps^2/km nominal dispersion and 6.3 m HI1060 fiber with 22.1 ps^2/km at 1050 nm. The net GVD was 0.153 ps^2. The 45°-TFG-based NPR technique was employed as a mode locker to generate the dissipative soliton pulses.

The stable mode-locking state was achieved when the pump power reached the threshold of 196 mW. Figure 14(a) shows the optical spectrum with 9 nm FWHM at the central wavelength of 1050 nm. The steep spectrum profile edges are caused by the effect of gain spectral filtering and the physical filter bandwidth. The uniform pulse train measured by an oscilloscope with pulse–pulse separation of 33.7 ns (see in Figure 14 (b) and the radio frequency (RF) show that the mode-locked laser was working under fundamental mode with 29.646 MHz repetition rate, which is in good agreement with the value calculated from the total cavity length. The RF spectra in the range of 300 MHz bandwidth have shown there is no Q-switching or harmonic solitons. Figure 14(d) represents the pulse profile and phase in temporal domain, in which the pulse duration evaluated from the Gaussian fit is around 4 ps. The TBP of around 10 and parabolic phase profile indicated that the pulses have positive linear chirp. The DOP of output pulse was also measured around 26 dB, which indicated the output pulse was nearly single polarization state [10].

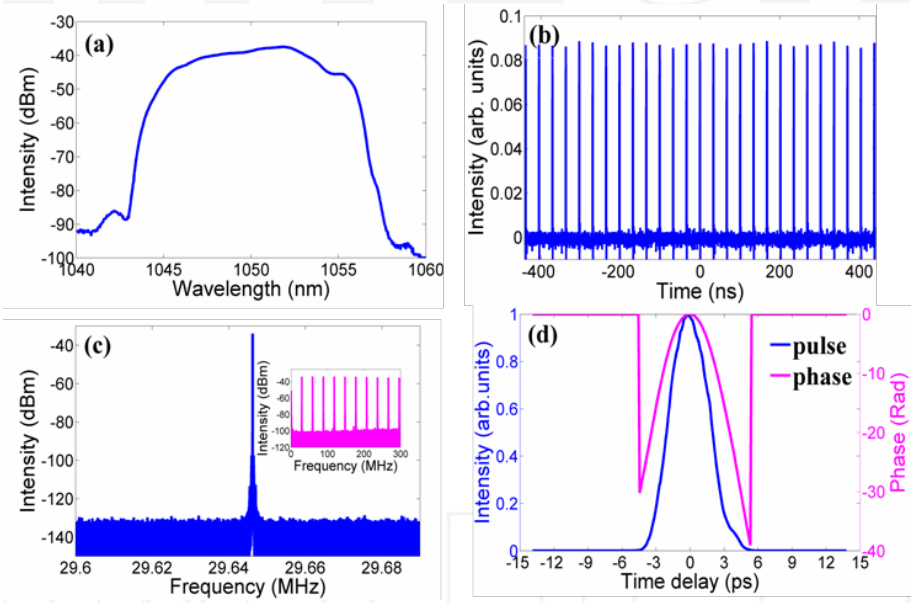

Figure 14. Characteristics of a 45°-TFG-based dissipative soliton YDF mode-locked fiber laser: (a) the optical spectra, (b) pulse train measured by an oscilloscope, (c) radio frequency spectra and (d) pulse duration and phase profile of output pulse at 196 mW pump power[10].

3.3.2. Bound-state mode-locked fiber laser

Soliton mode-locked lasers with multiple pulse output have attracted more interests in optical communications, plasma accelerators, and cosmetic surgery. There are two main operation regimes to generate multiple pulses: soliton interaction [45] and pulse splitting [46]. The former has been investigated for the limitation of soliton application in long-distance fiber optic

http://dx.doi.org/10.5772/61739

communications. As for specific multiple-pulse solitons, the bound-state solitons have fixed and discrete soliton separations, which have been extensively investigated in anomalous dispersion EDF-based fiber laser systems. Recent research work has shown that the bound-state solitons also exist in the normal-dispersion lasers. Ortaç et al. have reported a two-soliton molecule in an all-polarization-maintaining YDF fiber laser operating in the normal dispersion regime [47]. The bounded dissipative pulses in 45°-TFG-based all-fiber YDF laser were also observed [11], in which the design of laser cavity is the same as the one described in the previous section (see in section 3.3.1). Using the coupled Ginzburg–Landau equation (GLE) model, the theoretical analysis has indicated that the dissipative pulses in the normal dispersion domain also follow the energy quantization effect. The mechanism of formation of multiple pulse is based on soliton interaction through the dispersive waves in the all-normal dispersion region, in which the dispersive waves with discrete spectra can be generated when the propagating soliton in the laser cavity experiences periodical loss and amplification. In this YDF laser, the physical filtering of isolator also plays a critical role in the formation of bound-state pulses. Due to the soliton energy quantization effect, the bound-state solitons have the identical parameters, that is, the peak-to-peak separation is fixed and will not change with the pump power.

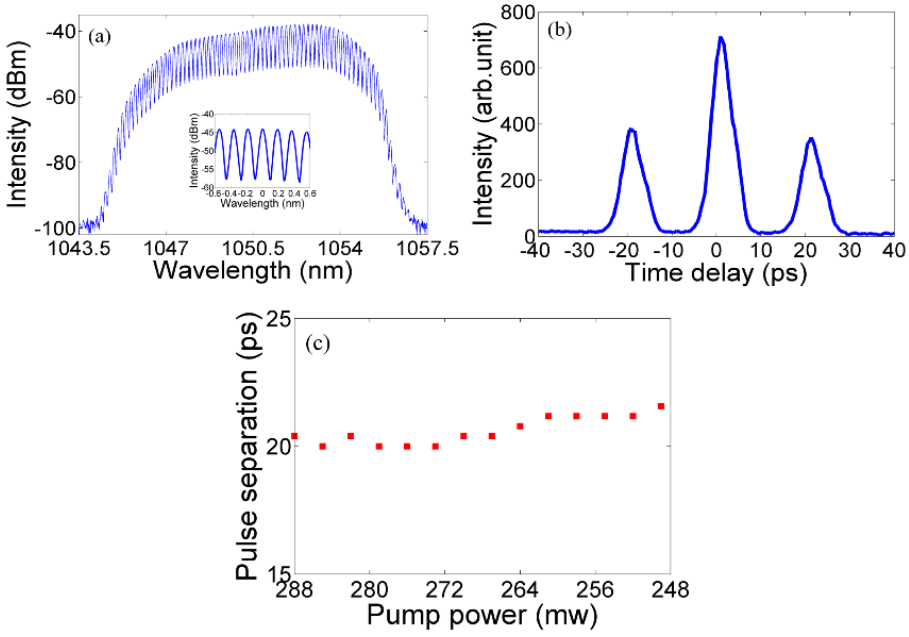

Figure 15. (a) Optical spectrum and (b) autocorrelation trace of bound-state dissipative mode-locked laser at pump of 249 mW; (c) the pulse separation influence as the pump power changes from 288 mW to 249 mW[11].

Since the dispersive waves in a laser system are pump strength dependent, by increasing the pump power, stable bound-state pulses could be formed. In the experiment, when the pump power reached to 214 mW, the stable single pulse was first generated by adjusting the PCs. After the pump power increased to 260 mW, the bound-state pulses (multiple pulses) were observed, which resulted from the peak power clapping effect under the stronger pump power. Once the formation of multiple pulses was established, by changing the pump power between 249 mW and 288 mW, the bound state of the pulses was still sustained. Reducing the pump power to 249 mW, the laser output reverted to the stable single pulse, and increasing the pump power above 288 mW, the laser operation evolved to CW regime. A pump power of 249 mW was verified as the threshold for bound-state pulse operation in this laser configuration. Figure 15(a) shows the output spectrum of bound-state pulse at the pump power of 249 mW. The pulse duration trace is shown in Figure 15(b), in which the Gaussian shape fitted pulse has a 4.2-ps duration and 21.6-ps separation (5 times larger than the pulse duration). As shown in Figure 15(b), three pulse peaks with a height ratio of 1:2:1 indicate that there are two identical bound-state pulses. By changing the pump power between 249 mW and 288 mW, the pulse separation remains almost unchanged as shown in Figure 15(c)).

3.3.3. Dual-wavelength mode-locked fiber laser at 1 μm

As shown in Figure 13(b), the 45°-TFG with central response around 1μ m also has a very broad PER profile. By using a 45°-TFG in the ring cavity, a dual-wavelength YDF mode-locked fiber has also been demonstrated [14]. The configuration of this dual-wavelength fiber laser consists of a segment of 45°-TFG in HI1060 fiber, a 980/1053-nm wavelength-division-multiplexed (WDM) coupler, a 0.73-m-long YDF with an absorption coefficient of 500 dB/m at 976 nm and 20 ps^2/km, an OC)with 30% output, two PCs, and 5.57-m HI1060 fiber with 22.1 ps^2/km at 1050 nm. The net GVD of the cavity is ~0.14 ps^2, which indicates the laser working in the dissipative regimes.

The stable self-started dual-wavelength mode-locked dissipative soliton was easily obtained by adjusting two PCs at a pump power higher than the mode-locking threshold. Figure 16(a) clearly shows the spectrum of the dual-wavelength mode-locked laser at the pump power of 339 mW, in which the two-peak central wavelengths are at 1033 nm and 1053 nm with approximately 10 nm FWHM. Due to the different round trip times, the dual-wavelength pulses have different repetition rates. The pulse train spectra of dual-wavelength pulse measured by a 6-GHz bandwidth oscilloscope had a very slightly different separation, making it difficult to measure the pulse train gap difference. As shown in Figure 16(b), there are two pulse trains, when one pulse train is triggered, the other is still moving. The uniform intensity pulse train shown in Figure 16(b) denotes that the dual-wavelength pulses have equal pulse energy. The RF spectrum in Figure 16(c) shows clearly that the dual-wavelength mode-locked laser has a 6-kHz difference of fundamental repetition rate, as one pulse at 1033 nm has 32.804 MHz repetition rate and the other at 1050 nm has 32.798 MHz repetition rate (see in Figure 16(c). The 65-dB SNR measured from RF spectrum indicates the laser was working at stable mode-locked state. The average power of pulse was 31 mW under 339 mW pump power. To further confirm pulse performance, the output port was connected with a filter to filter out the

http://dx.doi.org/10.5772/61739

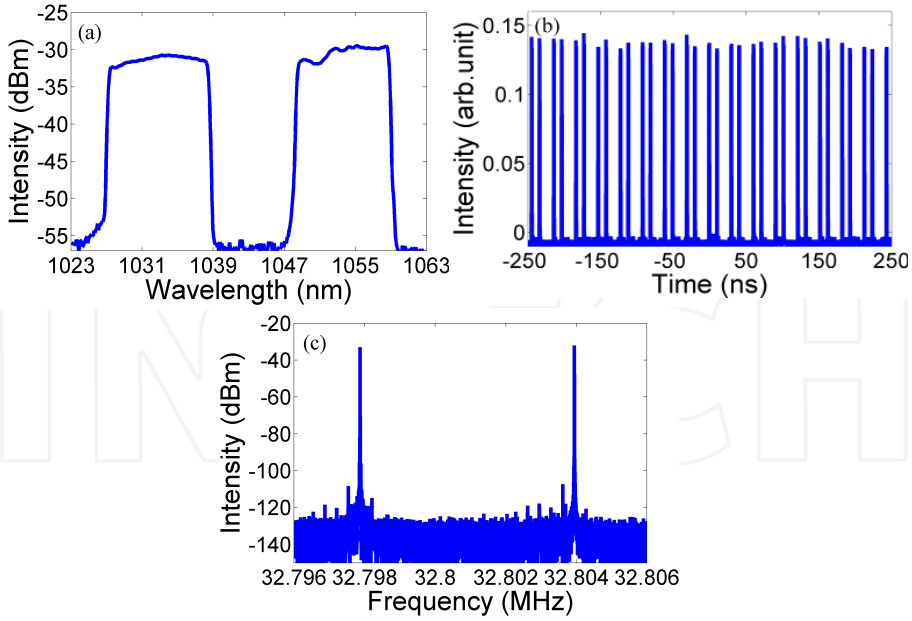

Figure 16. (a) Output spectrum, (b) oscilloscope trace, and (c) RF spectrum of dual-wavelength mode-locked laser at 1μ m [14].

pulse at 1033 nm. The optical spectrum, pulse train in oscilloscope, and RF spectra corresponding to the pulse at 1033 nm all disappeared, only the ones for the 1053-nm pulse remained, as can be seen in Figures 17(a), (b), (c). The average pulse power at 1053 nm measured was 15 mW, which is half of the dual-wavelength pulse power, further proving that the two pulses have the same pulse energy. The pulse duration shown in Figure 17(d) is ~4.3 ps fitted with Lorentz shape, and the corresponding TBP of pulse is calculated as 12.5, indicating that the pulse is highly chirped.

Through further investigation, it was observed that the dual-wavelength pulse laser was only sustainable at the pump power between 339 mW and 389 mW. Once the pump power increased to above 389 mW, the operation at short wavelength became CW. With further increase in pump power to 441 mW, the CW emission totally ceased and the fiber laser operated in stable single-wavelength mode locking [14].

3.4. 45°-TFG-based mode-locked fiber laser at 2 μm

Recently, as several types of thulium-doped fiber (TDF) are available, the all-fiber mode-locked fiber lasers have attracted increasing interest in the 2-μm region, as mid-IR fiber lasers are desirable not only for military applications in guidance and light detection and ranging (LIDAR) systems, but also for civil applications in biology, remote gas sensing, and free-space communication. Ultrafast fiber laser at 2 μm also serves as the seed source to generate the

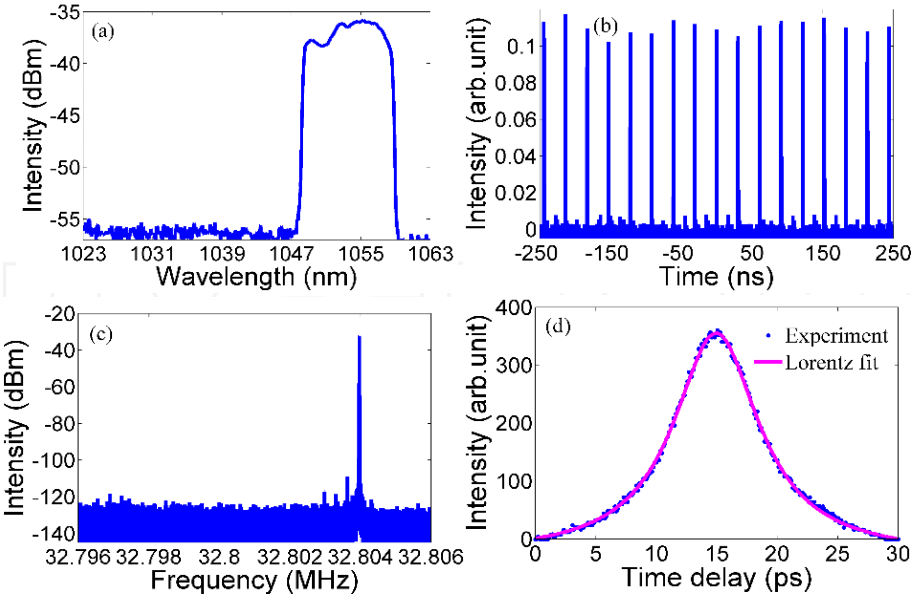

Figure 17. (a) the output spectra, (b) pulse train, (c) radio frequency and (d) autocorelation of output dual-wavelength pulse after a 1033-nm filter [14].

supercontinuum in the mid-IR region. There are a good number of reports on 2-μm mode-locked fiber lasers utilizing nanomaterial-based SA, NOLM, and NPR techniques [13, 48, 49]. Sun et al. have recently reported the fabrication of FBGs and 45°-TFGs in the 2-μm region. Figure 18 shows that a 25-mm-long 45°-TFG with 980-nm period has a strong PER response with FWHM over 400 nm and a peak value of PER around 25 dB at the central wavelength of 2 μm. By using the 45°-TFG-based NPR technique, Li et al. have demonstrated a TDF fiber mode-locked laser working at conventional soliton and noise-like soliton regimes [13].

The ring cavity of TDF laser emitting light around 2μ m reported by Li et al. has a total of 105-m-long cavity length, constructed by 7-m double-clad Tm^{3+}-doped fiber (Coractive, DCF-TM-10/128) with –84 ps^2/km at 2 μm, 95.0-m SM2000 fiber with –84 ps^2/km, and 3.0-m SMF-28e pigtail fiber from the pump combiner, isolator, and coupler estimated to be −80 ps^2/km. The use of 95-m SM2000 is to increase the nonlinearity of the cavity as the 2-μm fiber has a low nonlinear coefficient. The fiber combinations give a total net GVD of ~−7.76 ps^2, indicating this laser is operating at a large anomalous dispersion. The TDF 2-μm laser was pumped by two 793-nm diode lasers (Lumics, Germany) combined by a (2 + 1) × 1 pump combiner (ITF, Canada).

3.4.1. Conventional soliton mode locking

The conventional soliton results from the balance between nonlinearity and dispersion of laser cavity. The optical fiber at 2 μm has relatively low nonlinear coefficient. To enhance the

http://dx.doi.org/10.5772/61739

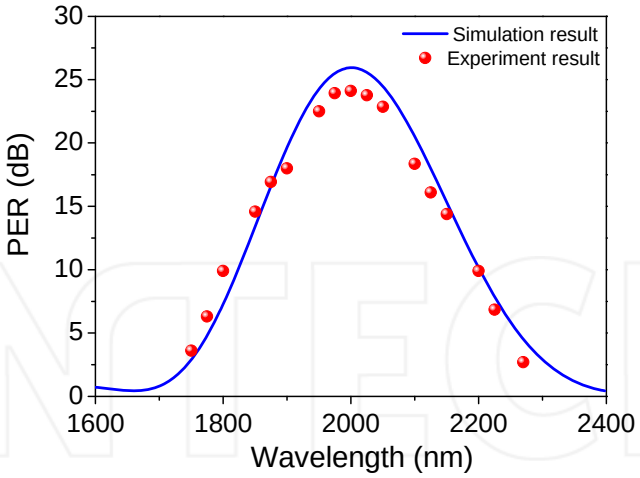

Figure 18. Measured (dot) and simulated (line) PER profile of 45°-TFG with a broad response at the 2-μm region [13].

nonlinear effect of laser cavity, the laser system, as mentioned above, has employed extra 95-m SM2000 in the ring cavity. However, due to the anomalous dispersion of active and passive fibers at 2 μm, the net GVD of the laser cavity is quite large.

During the experiment, the stable single pulse was not self-started, and the laser was first operating at multi-pulse mode-locking regime at the pump power of 1.320 W. Upon reducing the pump power to 1.232 W, a stable single-pulse mode-locked output was achieved. In the experiment, it was found that the single-pulse mode locking was working at a very narrow pump power range between 1.230 W and 1.232 W. Below 1.230 W, the laser operation evolved to CW regime, while above 1.232 W, the laser came back to multi-pulse operation. Figure 19(a) shows the output spectrum under single-pulse operation. As shown in the figure, there are very strong Kelly sidebands on the soliton spectrum, and the intensity of +/–1 sideband is even higher than the intensity of center value of the soliton. The Kelly sidebands are generated from the interference between the soliton and dispersive waves and usually exist in the fiber laser system associated with high dispersion and nonlinearity. The appearance of strong Kelly sidebands also indicates that the pulse duration may be close to the minimum possible value. The pulse train recorded by oscilloscope is shown in Figure 19(b). The fundamental repetition rate of mode-locked pulse was measured at 1.902 MHz by an RF spectrum analyzer, which matches well with the theoretically cavity length dependent value, and also indicates only one pulse was generated per round trip (see in Figure 19(c). Figure 19(d) displays the autocorrelation trace of the mode-locked pulses with a scanning range of 10 ps, in which the FWHM is about 3.4 ps corresponding to the pulse duration of 2.2 ps when using sech^2-pulse fitted. According to 2.2-nm FWHM of the optical spectrum of soliton mode-locked laser at central wavelength of 1992.7 nm, the TBP is calculated to be around 0.335, which is almost the transform-limited value (0.315 for sech^2 shape pulse).

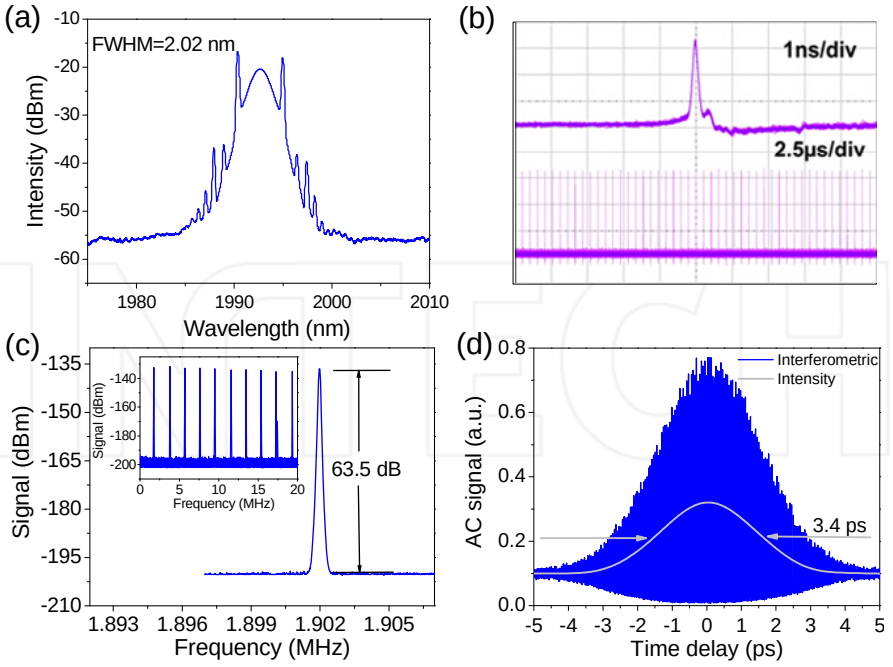

Figure 19. Thulium-doped fiber-based mode-locked fiber laser at conventional soliton regime: (a) output optical spectrum; (b) pulse train on oscilloscope; (c) RF spectrums with scanning range of 10 kHz to 20 MHz (inset); (d) intensity of autocorrelation with sech2-pulse fitting [13].

3.4.2. Noise-like mode locking

In contrast to the stable soliton mode-locked laser, the noise-like mode-locked laser emits a group of pulses with randomly varying duration and peak power, which was first reported by Horowitz et al. in 1997 [50]. The feature of low coherence length and broad spectral bandwidth of noise-like pulse lasers may make them useful for optical spectrum slicing and fiber optical sensing. Due to the weak distortion after propagating in the dispersion medium, the noise-like pulse may also be utilized for supercontinuum generation [51].

Li et al. observed noise-like pulse emission from the stable soliton mode-locked laser when the pump power increased to 1.82 W. The autocorrelation trace they observed showed a narrow peak riding on a broad pedestal extended over 150-ps measurement window, as shown in Figure 20(a). The relative broad and smooth output spectrum of noise-like pulse shown in Figure 20(b) reveals the central wavelength is at 1994.2 nm and FWHM is quite broad, around 18.1 nm. Both output and autocorrelation trace have indicated clearly the laser operates at the noise-like mode-locked regime. The RF spectrum has shown a repetition rate of 1.902 MHz, which proves the noise-like pulse operated at the fundamental mode-locking regime. Comparing with the stable soliton mode-locked laser, the noise-like laser showed a lower SNR around 47.3 dB. The noise-like mode-locking state could be still sustained at the maximum

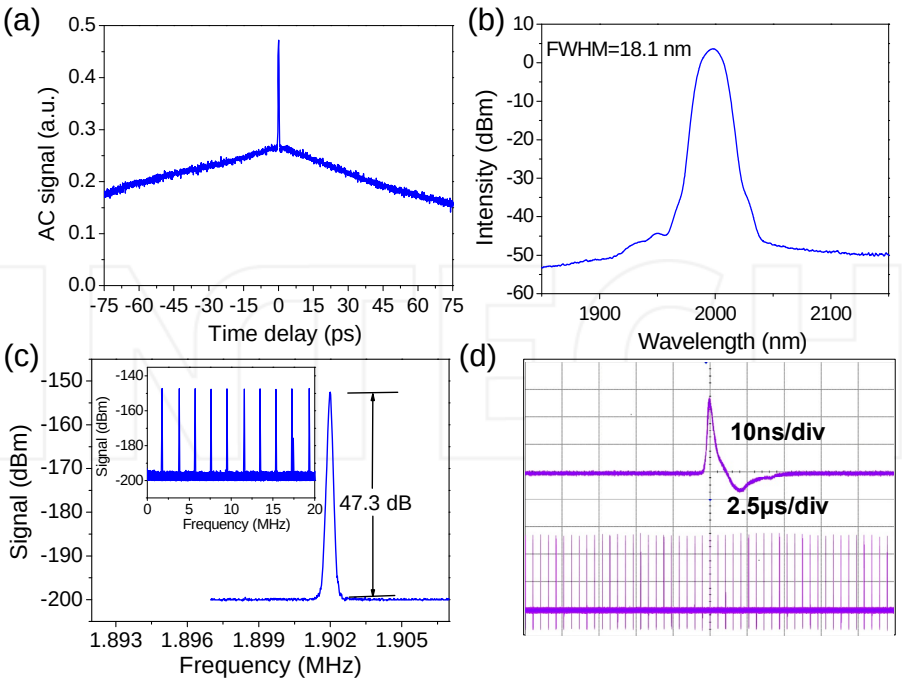

Figure 20. Thulium-doped fiber-based mode-locked fiber laser operating at the noise-like regime: (a) autocorrelation trace; (b) optical spectrum; (c) RF spectra; (d) output pulse train recorded by oscilloscope [13].

launched pump power of 7.56 W with a 7.5% slope efficiency and the maximum output power of 475.8 mW, corresponding to 250.1 nJ pulse energy. Such high pulse energy could be used to generate mid-IR supercontinuum.

Overall, the above-described mode-locked lasers at 2 μm have shown good stability under laboratory conditions within 24 hours. Further investigation of cavity length has revealed that adding or reducing the length of SM2000 fiber has not improved the condition to revert to soliton state mode locking. In fact, upon reducing the SM2000 fiber length from 95 m to 85 m, even higher pump power was required to generate noise-like pulses, while increasing the SM2000 fiber length to 120 m, the laser system was operating at the CW regime and no longer supported the mode-locking regime[13].

4. Summary and future work

In summary, we have presented the detailed theory, fabrication, and characterization of 45°-TFGs, which reveal clearly their high polarization function. 45°-TFGs as ideal in-fiber polarizers have many advantages, such as high PER performance, broad working bandwidth, low insertion loss, and high handling power. We have also reviewed the recent achievements of

applications of 45°-TFGs in all-fiber ultrafast fiber lasers at three distinctive wavelength ranges (1 μm, 1.5 μm, and 2 μm) operating in different mode-locking regimes. For future applications, we foresee that 45°-TFGs may be utilized in fiber laser systems to extend the operation wavelength to visible and deeper mid-IR range. One significant property of 45°-TFGs is their fiber compatibility and low insertion loss; thus they could be suitable in-fiber devices for high power all-fiber ultrafast laser systems. Overall, we expect the 45°-TFG-based fiber laser systems to play an important role to generate frequency comb and multi-wavelength operation for potential applications in high-speed optic communications, gas and environment sensing, social security, and medical diagnosing and treatment systems.

Author details

Zhijun Yan[1,2*], Chengbo Mou[1], Yishan Wang[2], Jianfeng Li[3], Zuxing Zhang[4], Xianglian Liu[5], Kaiming Zhou[1,2] and Lin Zhang[1]

*Address all correspondence to: yanz3@aston.ac.uk

1 Aston Institute of Photonic Technologies (AIPT), School of Engineering and Applied Science, Aston University, Aston Triangle, Birmingham, United Kingdom

2 State Key Laboratory of Transient Optics and Photonics, Xi'an Institute of Optics and Precision Mechanics, Chinese Academy of Sciences, Xi'an, China

3 State Key Laboratory of Electronic Thin Films and Integrated Devices, School of Optoelectronic Information, University of Electronic Science and Technology of China (UESTC), Chengdu, China

4 School of Optoelectronic Engineering, Nanjing University of Posts and Telecommunications, Nanjing, China

5 Key laboratory of Advanced Transducers and Intelligent Control system, Ministry of Education, College of Physics and Optoelectronics, Taiyuan University of Technology, Taiyuan, China

References

[1] Miniscalco, W.J.. Erbium-doped glasses for fiber amplifiers at 1500 nm. Journal of Lightwave Technology. 1991;9 (2): 234–250.

[2] Kawasaki, B.S., Hill, K.O., Lamont, R.G.. Biconical-taper single-mode fiber coupler. Opt. Lett. 1981;6 (7):327–328.

[3] Lee, B.. Review of the present status of optical fiber sensors. Optical Fiber Technology. 2003;9 (2):57–79.

[4] Rao, Y.J.. In-Fibre Bragging grating sensors. Meas. Sci. Technol. 1997;8:355–375..

[5] Bennion, I., Williams, J.A.R, Zhang, L., Sudgen, K., Doran N. J.. UV-written in-fibre Bragg gratings. Optical and Quantum Electronics. 1996;28 (2):93–135.

[6] Kaiming Zhou, G.S., Xianfeng Chen, Lin Zhang, Ian Bennion. High extinction ratio in-fiber polarizers based on 45° tilted fiber Bragg gratings. Opt. Lett.. 2005;30 (11): 1285–1287.

[7] Yan, Z., Mou, C., Chen, X., Zhou, K., Zhang, L.. UV-Inscription, Polarization-Dependant Loss Characteristics and Applications of 45°Tilted Fiber Gratings. J. Lightwave Technol. 2011;29 (18):2715–2724.

[8] Chengbo Mou, Kaiming Zhou, Lin Zhang, Ian Bennion. Characterization of 45°-tilted fiber grating and its polarization function in fiber ring laser. Journal of Optical Society of America. 2009;26 (10):1905–1911.

[9] Mou, C., Wang, H., Bale, B.G., Zhou, K, Zhang, L, Bennion, I. All-fiber passively mode-locked femtosecond laser using a 45°-tilted fiber grating polarization element. Optics Express. 2010;18 (18):18906–18911.

[10] Liu, X., et al.. All-fiber normal-dispersion single-polarization passively mode-locked laser based on a 45°-tilted fiber grating. Optics Express. 2012;20 (17):19000–19005.

[11] Xianglian, L., et al.. Bound dissipative-pulse evolution in the all-normal dispersion fiber laser using a 45° tilted fiber grating. Laser Physics Letters. 2013;10 (9):095103.

[12] Zhang, Z., et al.. Sub-100 fs mode-locked erbium-doped fiber laser using a 45 degree-tilted fiber grating. Optics Express. 2013;21 (23):28297–28303.

[13] Li, J., et al.. Thulium-doped all-fiber mode-locked laser based on NPR and 45° tilted fiber grating. Optics Express. 2014;22 (25):31020–31028.

[14] Xianglian, L., et al.. Single-polarization, dual-wavelength mode-locked Yb-doped fiber laser by a 45°-tilted fiber grating. Laser Physics Letters. 2015;12(6):065102.

[15] Zuxing, Z., et al.. All-fiber 250 MHz fundamental repetition rate pulsed laser with tilted fiber grating polarizer. Laser Physics Letters. 2015;12 (4):045102.

[16] Hill, K.O, Fujii Y., Johnson, D. C., Kawasaki, B.S.. Photonsensitivity in optical fibre waveguides: Application to reflection filrer fabrication. Appl. Phys. Lett.. 1978;32:647–649.

[17] G. Meltz, W.W.M., W.H.G. 1990. TuG1. In-Fibre Bragg grating tap. Optical Fibre Communications, San Francisco, California, USA, 1990 OSA Technical Digest Series 1. 1990;:TuG1.

[18] Williams, J. A. R., Sugden, I.B., K., Doran, N. J.. Fibre dispersion compensation using a chirped in-fibre Bragg grating. Electronics Letters. 1994;30:985–987.

[19] Ramachandran, S., Wang, Z., Yan, M.. Bandwidth control of long-period grating-based mode converters in few-mode fibers. Opt. Lett.. 2002;27 (9):698–700.

[20] Mihailov, S. J., R.B.W., Lu, P., Ding, H., Dai, X., Smelser, C., Chen, L.. UV-Induced polarisation-dependant loss(PDL) in tilted fibre Bragging gratings: application of a PDL equaliser. IEE Proc. Oproelectronics. 2002;149:211–216.

[21] Sipe, T.E., J.E.. Tilted fibre phase gratings. J. Opt. Soc. Amer. A. 1996;13:296–313.

[22] Brown, Y.L., T.G.. Radiation modes and tilted fiber gratings. Journal of Optical Society of America. 2006;23 (8):1544–1555.

[23] Yufeng Li, M.F., T.E.. Volume Current Method for Analysis of Tilted Fibre Gratings. Journa of Ligthwave Technology. 2001;19(10):1580–1591.

[24] Yoshino, T.. Theoretical analysis of a tilted fiber grating polarizer by the beam tracing approach. J. Opt. Soc. Am. B. 2012;29(9):2478–2483.

[25] G. Meltz, W.W.M., W.H.G.. Formation of Bragg Grating in optical fibres by a transverse holographic method. Optics letters. 1989;14:823–825.

[26] Hill, K.O., et al.. Photosensitivity in Eu2+ :Al2O3-Doped-Core Fiber: Preliminary Results and Application to Mode Converters. Optical Society of America. 1991;

[27] Hill, K. O., B.M., Bilodeau, F., Johnson, D. C., Albert, J.. Bragging gratings fabricated in monomode photosensitive optical fibre by UV exposure through a phase mask. Appl. Phys. Lett. 1993;62:1035–1037.

[28] Anderson, D. Z., V.M., Erdogan, T., White, A.. Production of in-fibre gratings using a diffractive optical element. Electron. Lett.. 1993;29:566–567.

[29] Mihailov, S. L., R.B.W., Stocki, T. J., Johnson, D. C.. Fabrication of tilted fibre-grating polarisation-dependent loss equliser. Electron. Lett.,. 2001;37:284–286.

[30] Technologies, A.. Polarization Dependent Loss Measurement of Passive Optical Components. Application Note. 2001;5988–1232EN.

[31] Yan, Z., Zhou, K., Zhang, L.. In-fiber linear polarizer based on UV-inscribed 45o tilted grating in polarization maintaining fiber. Opt. Lett.. 2012;37 (18):3819–3821.

[32] Tamura, K., Haus, H.A., Ippen, E.P. Self-starting additive pulse mode-locked erbium fibre ring laser. Electronics Letters. 1992;28:2226–2228.

[33] Bergh, R.A., Lefevre, H.C., Shaw, H.J.. Single-mode fiber-optic polarizer. Opt. Lett.. 1980;5 (11):479–481.

[34] Feth, J.R., Chang, C.L.. Metal-clad fiber-optic cutoff polarizer. Opt. Lett.. 1986;11 (6): 386–388.

[35] Bao, Q., et al.. Broadband graphene polarizer. Nat Photon. 2011;5(7):411–415.

[36] Okamoto, K., Hosaka, T., Noda, J.. High-birefringence polarizing fiber with flat cladding. Journal of Lightwave Technology. 1985;3 (4):758–762.

[37] Villanueva, G.E. Pérez-Millán, P.. Dynamic control of the operation regimes of a mode-locked fiber laser based on intracavity polarizing fibers: Experimental and theoretical validation. Opt. Lett.. 2012;37 (11):1971–1973.

[38] Zhang, Z., et al.. All-fiber mode-locked laser based on microfiber polarizer. Optics Letters. 2015;40(5):784–787.

[39] Tamura, K., et al.. 77-fs pulse generation from a stretched-pulse mode-locked all-fiberring laser. Optics Letters. 1993;18(13):1080–1082.

[40] Turitsyn, S.K., Bale, B.G. Fedoruk, M.P.. Dispersion-managed solitons in fibre systems and lasers. Physics Reports. 2012;521(4):135–203.

[41] Grelu, P. Akhmediev, N.. Dissipative solitons for mode-locked lasers. Nat Photon. 2012;6 (2):84–92.

[42] DeLoach, L.D., et al.. Evaluation of absorption and emission properties of Yb^{3+} doped crystals for laser applications. Quantum Electronics, IEEE Journal of. 1993;29(4):1179–1192.

[43] Payne, S.A., et al.. Ytterbium-doped apatite-structure crystals: A new class of laser materials. Journal of Applied Physics. 1994;76(1):497–503.

[44] Ruehl, A., et al.. Similariton fiber laser with a hollow-core photonic bandgap fiber for dispersion control. Optics Letters. 2007;32 (9):1084–1086.

[45] Smith, K., Mollenauer, L.F.. Experimental observation of soliton interaction over long fiber paths: discovery of a long-range interaction. Optics Letters. 1999;14(22):1284–1286.

[46] Ranka, J.K., Schirmer, R.W., Gaeta, A.L.. Observation of Pulse Splitting in Nonlinear Dispersive Media. Physical Review Letters. 1996;77(18):3783–3786.

[47] Ortaç, B., et al.. Observation of soliton molecules with independently evolving phase in a mode-locked fiber laser. Optics Letters. 2010;35 (10):1578–1580.

[48] Li, J., et al.. All-fiber passively mode-locked Tm-doped NOLM-based oscillator operating at 2-μm in both soliton and noisy-pulse regimes. Optics Express. 2014;22 (7):7875–7882.

[49] Solodyankin, M.A., et al.. Mode-locked 1.93 μm thulium fiber laser with a carbon nanotube absorber. Optics Letters. 2008;33 (12):1336–1338.

[50] Horowitz, M., Barad, Y., Silberberg, Y.. Noiselike pulses with a broadband spectrum generated from an erbium-doped fiber laser. Optics Letters. 1997;22 (11):799–801.

[51] Zaytsev, A., et al.. Supercontinuum generation by noise-like pulses transmitted through normally dispersive standard single-mode fibers. Optics Express. 2013;21(13):16056–16062.

INTECH